

Smart Shoe Force Sensor Development and Analysis for Walking Gait

by
Jingya (Lauren) Luo

Submitted to the Department of Mechanical Engineering
in Partial Fulfillment of the Requirements for the Degree of

Bachelor of Science in Mechanical Engineering

at the

Massachusetts Institute of Technology

June 2018

©2018 Jingya Luo. All rights reserved.

The author hereby grants to MIT permission to reproduce and to
distribute publicly paper and electronic copies of this thesis document
in whole or in part in any medium now known or hereafter created.

Signature redacted

Signature of Author:

Department of Mechanical Engineering

Signature redacted

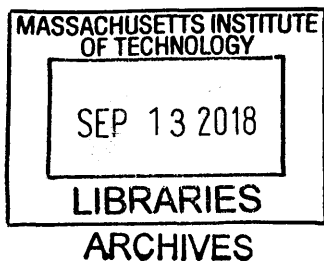
Certified by:

Sangbae Kim
Associate Professor of Mechanical Engineering
Thesis Supervisor

Signature redacted

Certified by:

Rohit Karnik
Professor of Mechanical Engineering
Undergraduate Officer





77 Massachusetts Avenue
Cambridge, MA 02139
<http://libraries.mit.edu/ask>

DISCLAIMER NOTICE

Due to the condition of the original material, there are unavoidable flaws in this reproduction. We have made every effort possible to provide you with the best copy available.

Thank you.

The images contained in this document are of the best quality available.

Smart Shoe Force Sensor Development and Analysis for Walking Gait

by
Jingya (Lauren) Luo

Submitted to the Department of Mechanical Engineering
on May 18, 2018 in Partial Fulfillment of the
Requirements for the Degree of

Bachelor of Science in Mechanical Engineering

ABSTRACT

Foot contact forces are imperative to gait analysis for uses such as elderly rehabilitation and athletic training. Previously developed methods for legged locomotion force detection involved convoluted sensing systems and significant external equipment. This thesis builds upon previous developed smart shoe sensors adapted from the MIT Cheetah robot using pressure sensors embedded in urethane rubber, Smooth-On's Vytaflex® 20. Past work developed accurate material models in Abaqus CAE to simulate foot contacts for compression and shear. This thesis builds upon the FEA models for two sensor sizes to create a simple model to measure torque and contact angle given force measured by the sensor. Using experiments with physical footpads on a CNC mill verified by simulations from Abaqus FEA, we derived models for contact angles between 0 to 15 degrees and rolling movement from -7 to 7 degrees at various compressions. Models successfully derive relationships between roll and contact angle versus force. These models can be used as a jumping point for data analysis using the smart shoe sensor.

Thesis Supervisor: Sangbae Kim
Title: Associate Professor of Mechanical Engineering

Acknowledgments

First, I would like to thank my thesis advisor Sangbae Kim and PhD candidate, Meng Yee (Michael) Chuah, for their direction and guidance on the project. Second, I would like to thank Juan Romero for helping with experimental setup, Iris Hwang and Wendy Ma for Abaqus Simulation debugging. I would also like to thank Fredrik Solberg for a resource for all Abaqus troubleshooting and Wei Li for teaching me how to automate Abaqus Simulation processes.

Table of Contents

Abstract	2
Acknowledgements	3
Table of Contents	4-5
List of Figures and Tables	6
1. Introduction	7
2. Background	7-8
2.1 Footpad Design	8
2.2 Footpad Material Model and Sensor Voltage Relationship	8-9
2.3 Contact Angle and Rolling Transition	9-10
3. Footpad Measure Setup	10
3.1 Experimental Setup	10-12
3.2 Abaqus Simulation	12
3.2.1 Simulation Modifications	13
3.2.2 Simulating Angled Compression	13
3.2.3 Simulation Rolling	13
4. Results and Discussion	13
4.1 Angled Compression	13-14
4.1.1 Large Footpad Experiment	14-15
4.1.2 Large Footpad Simulation	15-16
4.1.3 Large Footpad Experiment and Simulation Comparison	16-18
4.1.4 Small Footpad Experiment	19-20
4.1.5 Small Footpad Simulation	20
4.1.6 Small Footpad Experiment and Simulation Comparison	21-22
4.2 Rolling	23
4.2.1 Rolling Experiment	23-26
4.2.2 Rolling Simulation	26-27

4.2.3 Rolling Comparison and Curve Fit	27-28
5. Conclusions and Contribution	28-30
6. References	31

List of Figures and Tables

Table 2-1: Smart Shoe Footpad Dimensions	8
Figure 2-1: Heel Strike Gait Phase	10
Figure 3-1: CNC Mill Experimental Setup	11
Figure 3-2: Abaqus Footpad Mesh	12
Figure 4-1: Footpad Orientation	14
Figure 4-2: Large Footpad Sensor Voltage Output	15
Figure 4-3: Large Footpad Experiment and Simulation Comparison	16
Figure 4-4: Large Footpad Voltage to Force for All Angles	17
Figure 4-5: Large Footpad Force/Voltage to Angle with Trend Lines	17
Figure 4-6: Small Footpad Voltage to Force for All Angles	19
Figure 4-7: Large and Small Footpad Contact Surface Area Comparison	20
Figure 4-8: Small Footpad Force/Voltage to Angle with Trend Lines	21
Figure 4-9: Radial and Hoop Stress Diagram	22
Figure 4-10: Large and Small Footpad Vertical Stress Visualization	22
Figure 4-11: Roll Experiment Data	24
Figure 4-12: Sensor Voltage Difference to External Torque	25
Figure 4-13: Roll Behavior for All Angles	26
Figure 4-14: Roll Experiment and Simulation Comparison	27

1. Introduction

The design of a simple and robust method of analyzing gait force data is in high demand. Gait force data is a powerful tool for investigating posture and motor-motion affected diseases. For instance, clinical trials for Parkinson's use gait force profiles to monitor the effects of drugs [2]. Understanding the time and ground force reactions of gait components can deduce running speed, and this data is beneficial to athletic shoe design for minimizing injuries [3].

Current methods of studying gait force involves a combination of subjects running on large force plates and a camera for visual determination of joint kinematics [5]. While visual techniques have evolved, such methods involve heavy set up time, complexity in calibration, and is difficult to catch subjects in their natural environment.

Smart shoe footpads developed for this thesis has the advantage of being lightweight, robust, and close to location of action. To bring this product to market, models of analysis for sensor outputs are needed. Previous work characterized smart shoe footpad material properties, and derived a relationship between external contact force and sensor reading. There is, however, more to learn about sensor output behavior under various gait components.

2. Background

This thesis is built upon Studebaker's paper on *Material Modeling and Sensor Characterization for Optimizing Footpad Force*[1].

2.1 Footpad Design

The smart shoe developed by Chuah is composed of one large and four small cylindrical footpads molded with urethane rubber (Smooth - On's Vytaflex®20). Each footpad embeds four pressure sensors (Freescale's MPXH6400A) equidistant from the center. Table 2-1 displays the dimensions of footpads and the location of integrated pressure sensors.

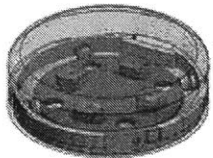

	Large Footpad(D65-H12)	Small Footpad(D45-H12)
		
Diameter (mm)	65	45
Height (mm)	12	12
Sensor Distance from Center (mm)	17.78	12.7

Table 2-1: Dimensions of smart shoe footpad and sensor location.

2.2 Footpad Material Model and Sensor Voltage Relationship:

Studebaker[1] found Odgen $n=2$ to be the optimal simulation material in Abaqus for the footpads, which he found by comparing simulation results with a hyper-elastic material model built from uniaxial tensile, uniaxial compression, planar tension, and volumetric compression tests. The relationship correlating sensor voltage outputs and simulation stress values are shown in Equation 2.1:

$$V_s = 1000 * \alpha * S22 + \beta \quad (2.1)$$

Where V_s is the sensor voltage, α is effective sensitivity, $S22$ is vertical stress in Abaqus simulation, and β is intercept adjustment factor. Effective sensitivity is correlated to aspect ratio of the footpad, using Equation (2.2):

$$\alpha = A + B * \left(\frac{d}{h}\right) \quad (2.2)$$

Where d is diameter of the footpad, h is height of the footpad, and A and B are coefficients determined to provide best match with experimental data. In Studebaker's study, $A = 10.633$, $B = 0.366$. The intercept adjustment factor varies with each footpad. These values are used as starting values for matching experimental and simulation data. The coefficients may change with different footpads due to manufacturing inconsistencies, and therefore each footpad should be calibrated accordingly.

2.3 Contact Angle and Rolling Transition:

A heel strike can be decomposed into two components: angled compression and rolling. Angled compression represents the scenario where forces are concentrated on one of four sensors embedded in the footpad. It occurs when the footpad engages the ground at a larger angle as shown in Figure 2-1a. Rolling involves the engagement of multiple pressure sensors, occurring at smaller contact angles, as shown in Figure 2-1b. Therefore, rolling is defined by the difference between pairs of sensor across from each other. A simulated heel strike will therefore be a sequence of angled compression, rolling, and angled compression again.

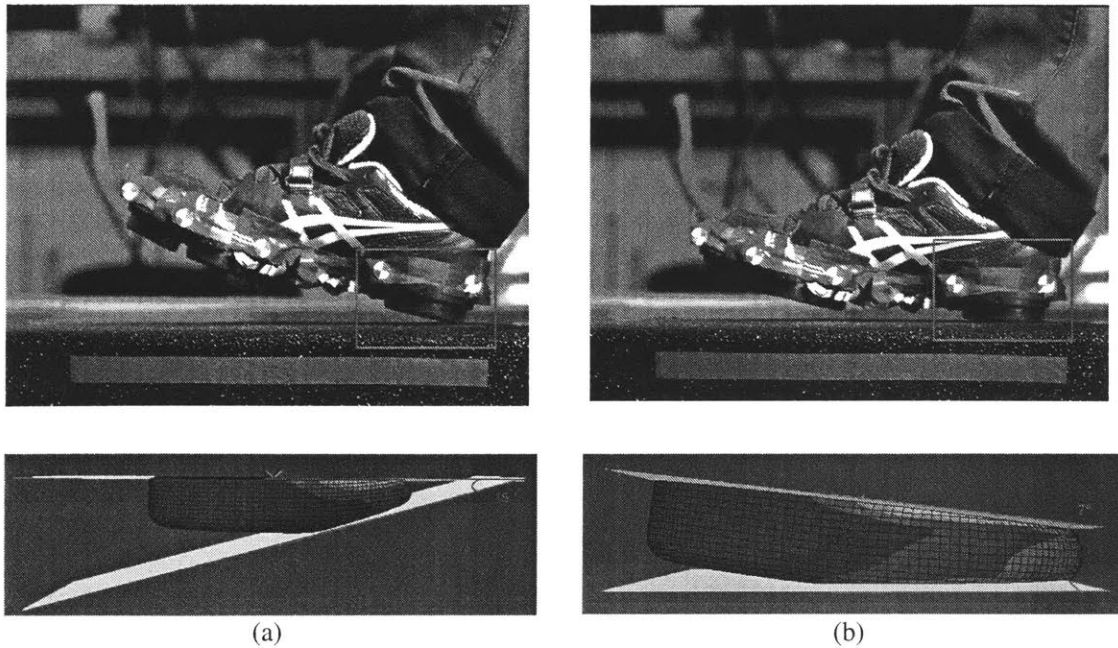


Figure 2-1: (a) Angled Compression in heel strike demonstrated with human wearing smart shoe sensor (above) compared to angle compression in simulation, showing a contact angle of 15 degrees. (b) Rolling in heel strike demonstrated by human wearing smart shoe sensor (above) compared to rolling in simulation, showing a contact angle of 7 degrees.

3. Footpad Measurement Setup

3.1 Experimental Setup:

To correlate force measurements with sensor readings, the testing method mentioned in Chuah et al. [6] is used. A 3-axis CNC mill (MicroMill DSLS 3000 from MicroProto Systems) is modified to include a 4th axis with a trunnion table capable of rotation. A 6-axis force/torque sensor (ATI Delta SI-660-60 from ATI Industrial Automation) mounted to the trunnion table measures true force. The sensor is mounted to the CNC mill spindle mount, and its position is controlled by CNC positioning code. Figure 3-1 shows this experimental setup with the sensor in contact with the 6-axis force/torque sensor. The CNC mill spindle mount positioning controls contact and

compression of the testing sensor, while the trunnion table attached to a rotary magnetic encoder (AEAT-6012 from Avago Technologies) controls rolling motion and angle of contact.

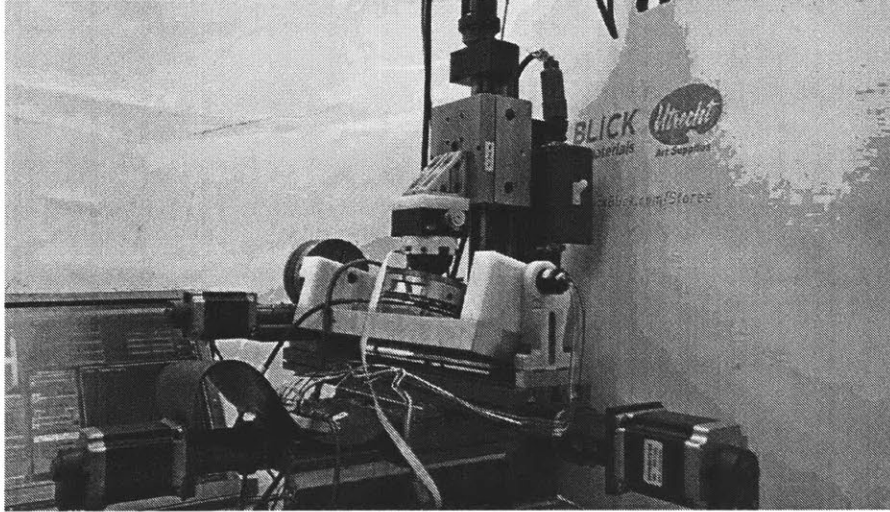


Figure 3-1: Experimental setup with CNC mill, footpad attached to CNC spindle mount, and a force sensor on the trunnion table.

Piezo-resistive sensor data are collected as 12-bit analog voltages SPI by a ARM Cortex-M4F microcontroller with a 1kHz sampling rate. Data from the 6-axis force/torque sensor are collected through a data acquisition system (CompactDAQ 9205 from National Instruments (NI)) at 1kHz. All data is synchronized using NI LabVIEW before analysis.

The following datasets were collected for both large (D65-H12) and small sensors (D45-H12):

1. Angled-Compression at 0 to 15 degrees, by increments of 1 degree, at compressions 0.5 to 4.5mm, by increments of 0.5mm.
2. Rolling with compression from -7 degrees to 7 degrees, at compressions 0.1mm, 0.2mm, 0.3mm, 0.4mm, 0.5mm, 0.75mm, 1mm, 1.25mm, 1.5mm, and 1.75mm.

3.2 Abaqus Simulation:

Abaqus CAE model files from Studebaker[1] is used with Odgen $n=2$ material model. The mesh is composed of structured hex elements separated into two sections: a rectangular section in the center of the sensor with corners at the location of pressure sensors embedded, and cylindrical section for the rest of the sensor. The rectangular section in the center is created to avoid warning from simulation. Figure 3-2 shows the model in Abaqus CAE. Data is analyzed using dynamic explicit method. Dynamic explicit method involves calculations updated at each time step increment. Small steps are taken until the final deformation or time specified is reached. This method is chosen because it is computationally efficient and has proven to be sufficiently accurate in Studebaker's experiments. Other methods were also explored, such as dynamic implicit method with hex-dominated sweep elements was used without the center rectangular partition. Dynamic implicit analysis is similar to dynamic explicit analysis except the next iteration step is predicted using Newton Raphson methods. While dynamically implicit analysis is capable of providing more stable and accurate results, it is also computationally and time intensive. As a result, it is used mostly for accurate visualizations.

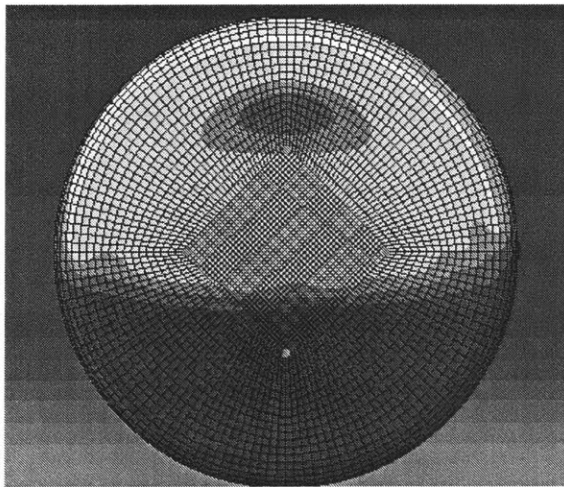


Figure 3-2: Footpad mesh, which is composed of a rectangular section in the center with corners at the location of the sensors. The rest of the sensor has cylindrical mesh.

3.2.1 Simulation Modifications:

From the original simulation files, the assemblies, boundary conditions, and steps are modified to match experimental methods. Velocities of simulation are chosen to ensure inertial effects are minimized in a quasi-static simulation such that dynamic components are mitigated. This is verified by ensuring kinetic energy is relatively small compared to inertial energy of the simulation. Stress and displacement results are independent of velocity of the simulation.

3.2.2 Simulating Angled Compression:

The bottom plate represents the ground, or in this case, the 6-axis force/torque sensor surface. To mimic an angled contact, the bottom plate is rotated by the tested angle. Figure 2-1a shows the testing assembly for a 15 degree contact angle. Compression step configuration and boundary conditions were maintained from Studebaker's model. Velocity of compression is 1 mm/s.

3.2.2 Simulating Rolling:

To simulate rolling motion, additional steps are created after compression with rotations of -0.122173 radians (-7 degrees), 0.244346 radians (14 degrees), and -0.122173 radians (-7 degrees) to mimic -7 to 7 degree rolling motion. The velocity of roll is $1 \frac{\text{degree}}{\text{s}}$.

4. Results and Discussion:

4.1 Angled Compression

Angled Footpad to ground contact data was procured through procedures mentioned in Section 3.1 for 120 different combinations of angles and compressions for both large and small footpad. Through these experiments, Studebaker[1]'s derived relationship between sensor voltage output

and external force value was used. A trend between angle of compression and voltage output was identified.

4.1.1 Large Footpad Experiment:

In angled compressions, one out of four sensors, sensor 3 in this orientation, experiences significantly more stress than other piezo-resistive sensors. Hence, sensor 3 voltage values strongly correlate with the reaction force measured by the 6-axis force/torque sensor. Figure 4-1 displays the orientation of the tested footpad and Figure 4-2 visualizes raw data collected from physical experiments. For all compressions, the maximum force and voltage pairs are extracted to form a relationship between footpad sensor voltage output and measured force. The relationship is generally linear, but the slope of the linear fit line varies with angle of compression, as depicted in Figure 4-4a.

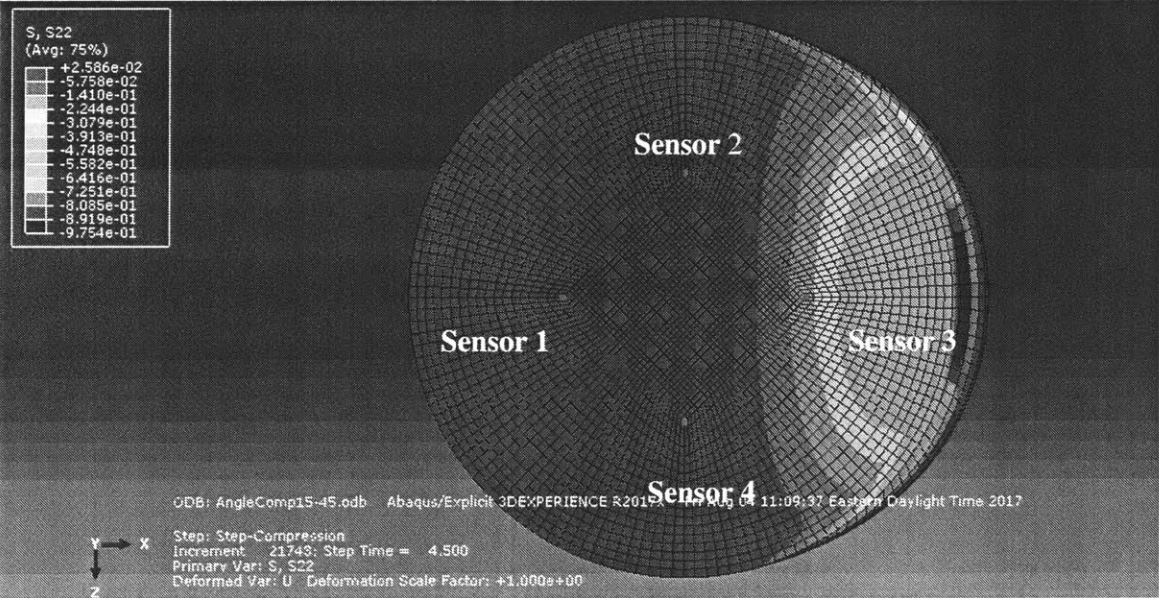


Figure 4-1: Abaqus simulation result demonstrating the orientation of sensor placement on a large footpad. The nodes in yellow, green, and blue demonstrate the portion of footpad with higher vertical stress forces, which overlaps significantly only with sensor 3.

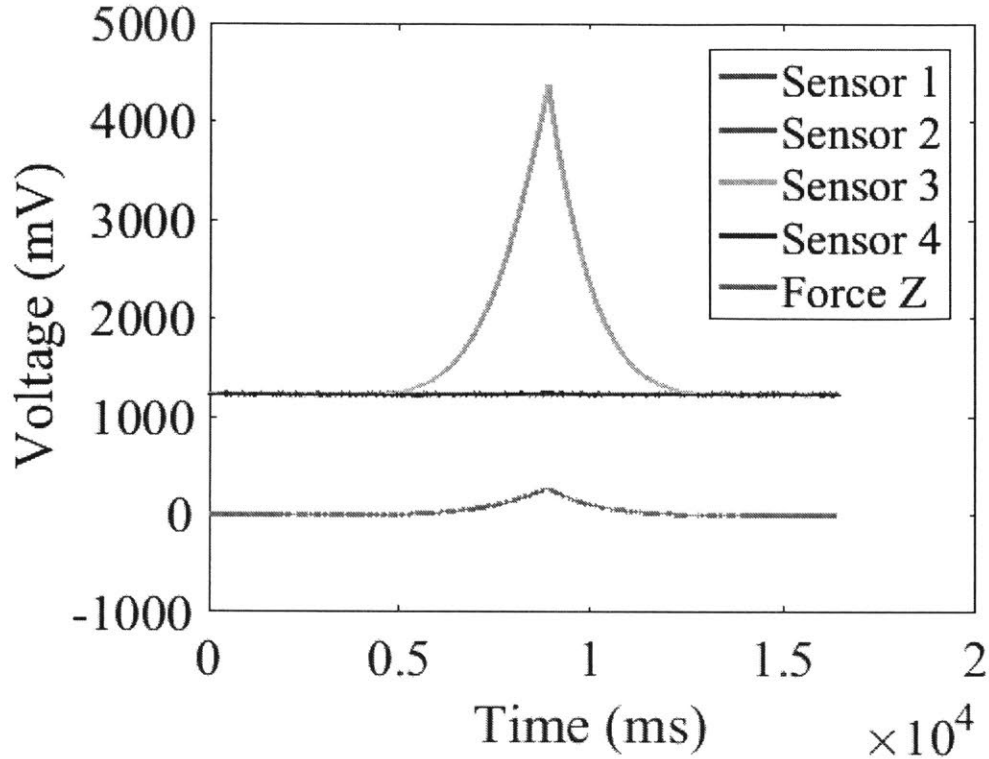


Figure 4-2: Data collected for angled compression at 15 degrees for 4.5mm compression. Sensor 3 displays a high voltage peak which corresponds to the peak in Force Z, force detected by 6-axis force sensor. Location of other 3 sensors have minimal vertical stress.

4.1.2 Large Footpad Simulation:

Similar to experimental results, one sensor in the footpad experiences significantly more vertical stress than the rest of the sensors. Therefore, the vertical stress of the most sensitive sensor is used in Equation 2-1 and 2-2 (Studebaker's equation) to create a comparable relationship between experimental and simulation data. Due to fabrication variation, Equation 2-2 parameters are adjusted for a better match. In this set of experiments, $A = 13.82$, $B = 0.356$, and $\beta = 1570$ for a large footpad with diameter of 65 mm and height of 12 mm. Figure 4-3 verifies this relationship is a good match for forces greater than 100 N.

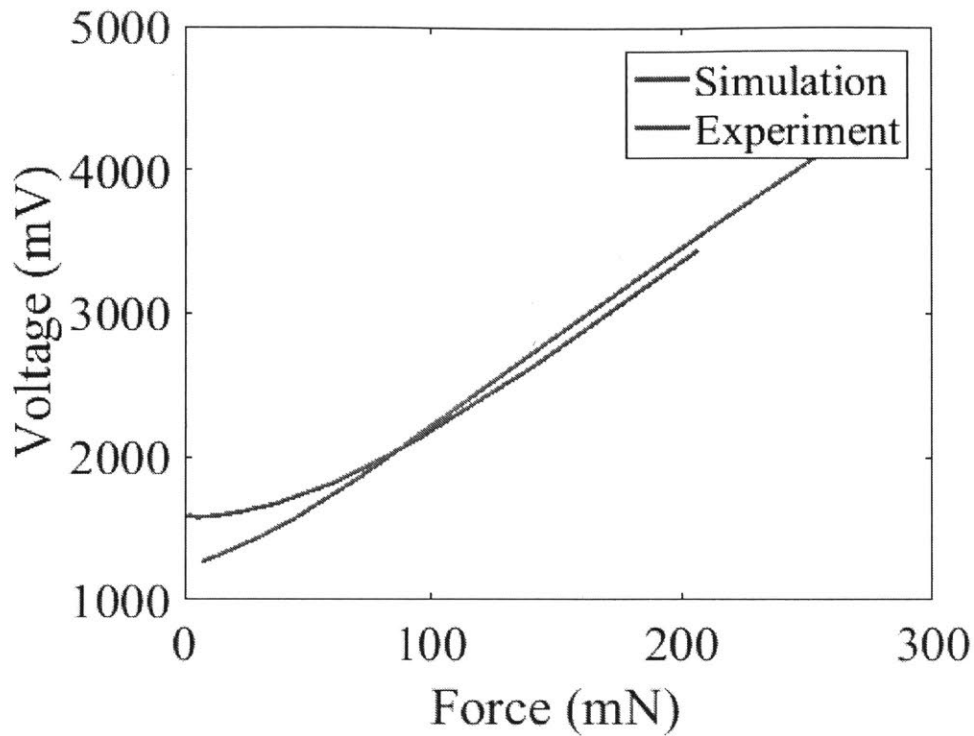


Figure 4-3: Comparison of simulation results to experimental results for large footpad angle compression at 15 degrees. Using the new fitted parameters ($A = 13.82, B = 0.356, \beta = 1570$) applied to Equation 2.1 and Equation 2.3, simulation and experimental results match well beyond 100 N.

4.1.3 Large Footpad Experiment and Simulation Comparison:

When modeling the sensor voltage output to external force for all angles 0 to 15 degrees, there is variation in gradient of the linear-like relationship as shown in Figure 4-4a and Figure 4-4b.

Figure 4-5 finds the characterizing slope for each angle and compares it across all angles for both experiment and simulation. In this case, the characterizing slope is the maximum gradient of the voltage to force relationship mentioned in Section 4.1.1 and depicted in Figure 4-4.

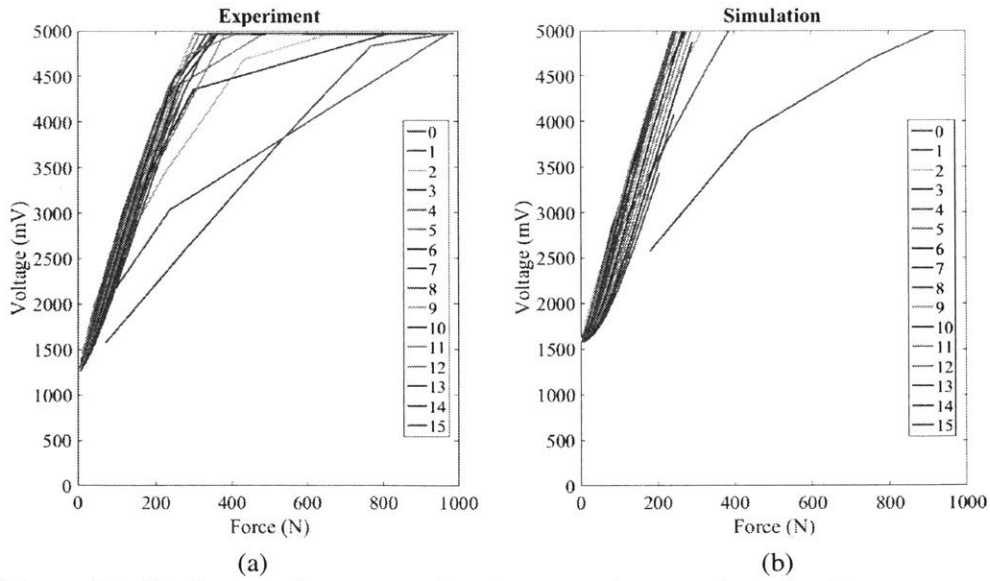


Figure 4-4: (a) Sensor voltage output for given ground contact force for all contact angles derived from experimental results. (b) Sensor voltage output for given ground contact force for all contact angles derived from simulation results.

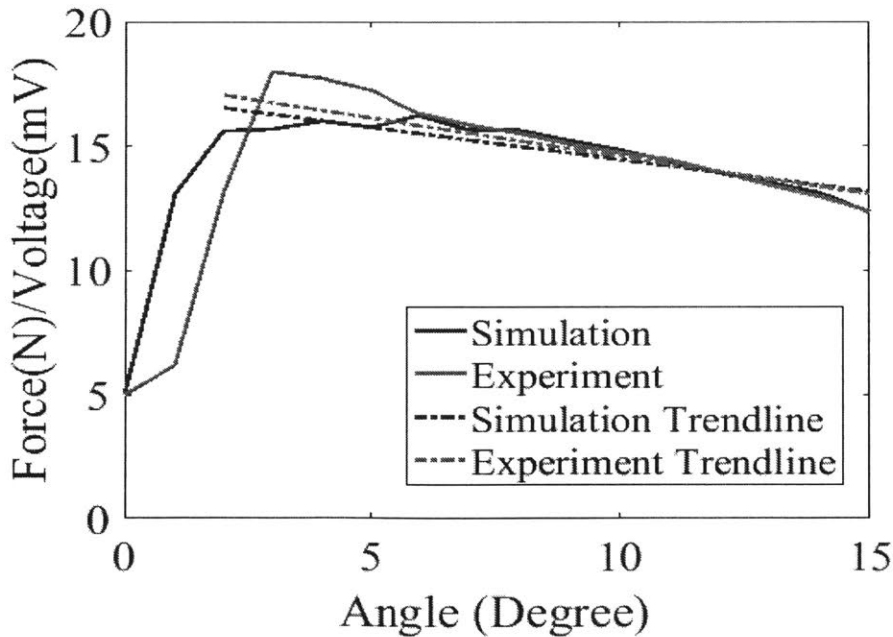


Figure 4-5: Force (N) to Voltage (mV) conversion factor compared to ground contact angle for both simulation and experimental results. Linear trend lines are fitted for both curves. Simulation has trend line of $\frac{Force}{voltage} [\frac{N}{mV}] = 17.054(\pm 0.740) - 0.259(\pm 0.079) * \varphi$ with R^2 value of 0.8103, and experiment has a trend line of $\frac{Force}{Voltage} [\frac{N}{mV}] = 17.662(\pm 1.790) - 0.306(\pm 0.191) * \varphi$ with R^2 value of 0.506, where φ is the contact angle. There is a close match for angles greater than 5 degrees.

Equation 4-1 and 4-2 are linear fitted trend lines between force/voltage to contact angle of simulation and experiment results.

$$\text{Simulation} \frac{\text{Force}}{\text{Voltage}} \left[\frac{N}{mV} \right] = 17.054(\pm 0.740) - 0.259(\pm 0.079) * \varphi \quad (4-1)$$

$$\text{Experimental} \frac{\text{Force}}{\text{Voltage}} \left[\frac{N}{mV} \right] = 17.662(\pm 1.790) - 0.306(\pm 0.191) * \varphi \quad (4-2)$$

φ is the contact angle. Simulation trend line has the property $R^2 = 0.8103$, and experiment trend line has the property $R^2 = 0.506$. The correlations defined by Equation 4-1 and 4-2 is more apparent in contact angles greater than 5 degrees. For lower degrees, there are inconsistencies in the collected data, observed by the flat portions of data curves in Figure 4-4a. This is due to sensors reaching sensing limits at low angles and high compressions and simulations not being quasi-static at low compressions. At smaller angle contacts (close pure compression), the method of analysis using one characterizing sensor is no longer applicable because force is distributed evenly amongst all four pressure sensors. A separate model for pure compression should be used for 0 degree contact, and rolling models should be used for smaller angles.

The negative relationship between force-voltage conversion and angle degree can be justified by the position of sensors and distribution of stress. At steeper angles (i.e. 15 degrees), sensors are further away from point of contact, therefore not sensing as much stress forces.

4.1.4 Small Footpad Experiment

Small sensors exhibit behavior similar to the large sensor where one out of four sensor experiences significantly more stress force. Therefore, one sensor is used to characterize the relationship between sensor voltage output and external reaction forces. Figure 4-6 compares voltage to force relationships of small footpads.

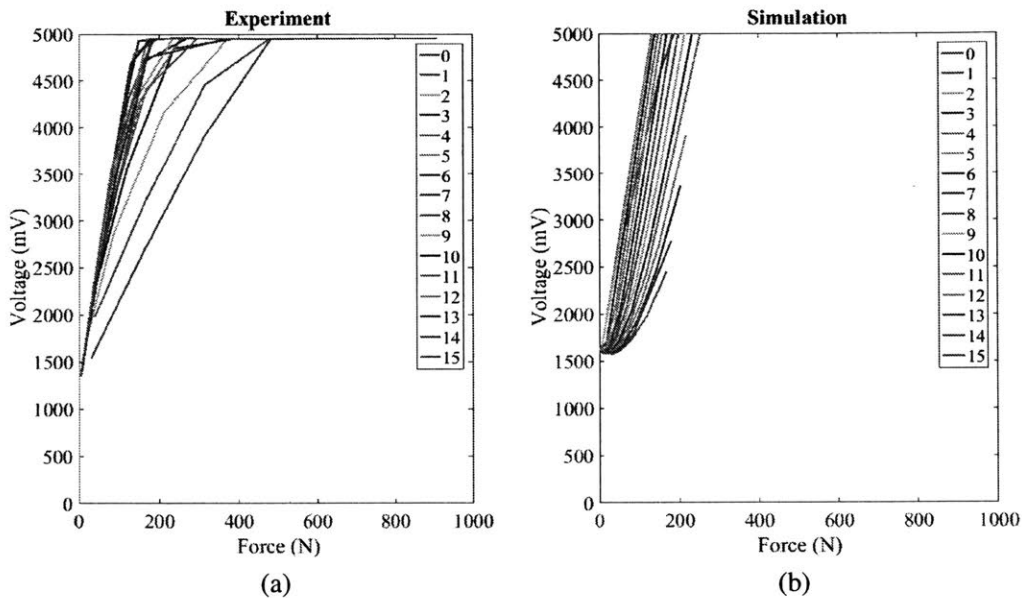


Figure 4-6: (a) Sensor voltage output for given ground contact force for all contact angles derived from experimental results. (b) Sensor voltage output for given ground contact force for all contact angles derived from simulation results.

Sensors in the small footpad have a higher voltage to force conversion, and reaches a sensing limit at a smaller force. In this set of experiments, small sensors reach limit at approximately 150N, which is significantly smaller than the limit of large footpad, which is approximately 300N. This is due to the difference in surface contact area between the large and small sensor, as demonstrated by Figure 4-7. Larger contact area correlates to a larger distribution of forces, hence less stress experienced by the individual sensors. This also leads to a smaller voltage output by the sensors given external applied force.

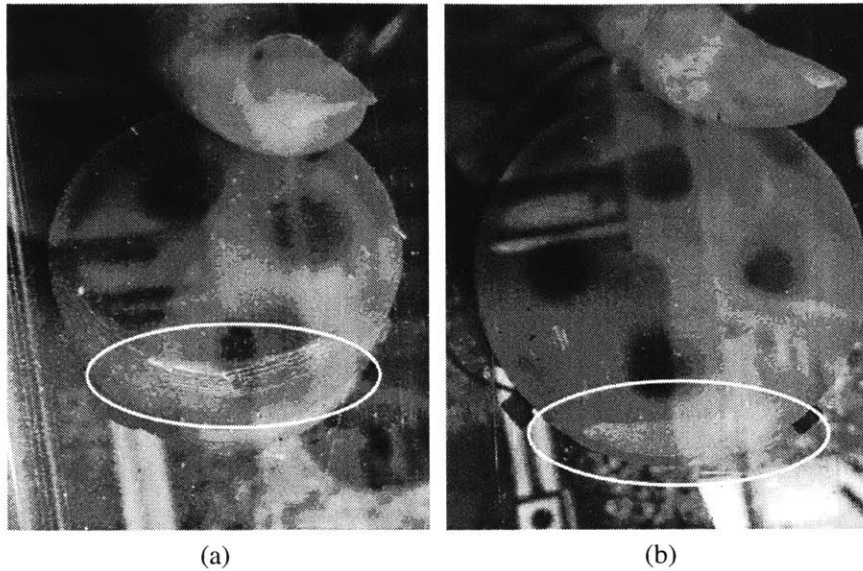


Figure 4-7: (a) Surface contact of small footpad is smaller than (b) surface contact of large footpad. The larger distribution of force on contact surface leads to less stress detected by pressure sensors, and results in a smaller voltage to force detection for large footpad.

4.1.5 Small Footpad Simulation

In simulation, the same higher voltage to force conversion for small footpad is carried over, as observed in Figure 4-6b. Simulation data for small footpad for various angle also exhibits a larger variation in gradient. This is because the sensors embedded in the small footpad are closer together, and as a result the sensors experience less distribution of stress amongst the four sensors at each angle. This is analogous to analyzing the smaller angles of large footpad data. The parameters applied to Equation 2.1 and 2.2 to convert simulation forces to sensor voltage are $A = 15$, $B = 5$, and $\beta = 1570$.

4.1.6 Small Footpad Experiment and Simulation Comparison

When attempting to derive a model between force-voltage gradient and footpad contact angle, as previously done with the large footpad, discrepancy is found between experimental and simulation data, as shown in Figure 4-8.

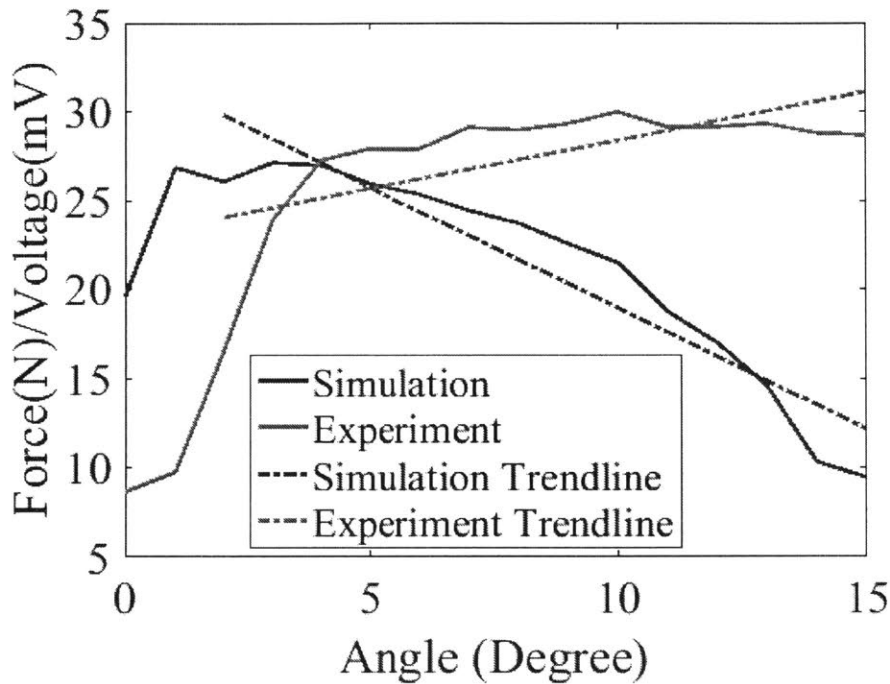


Figure 4-8: Force(N) to Voltage(mV) conversion factor compared to ground contact angle for both simulation and experimental results of small footpad. A linear trend line is fitted for both curves, however there is a disagreement in trend line behavior.

While simulation data displays a similar negative linear correlation between force/voltage and contact angle, experimental results does not show agreement. One hypothesis for the cause of the phenomenon is the location of sensor is close in proximity to a radial to hoop stress-force transition point. Modeling the footpad as a cylinder, the footpad experiences radial stress near the center and hoop stress around the edges, as depicted by Figure 4-9.

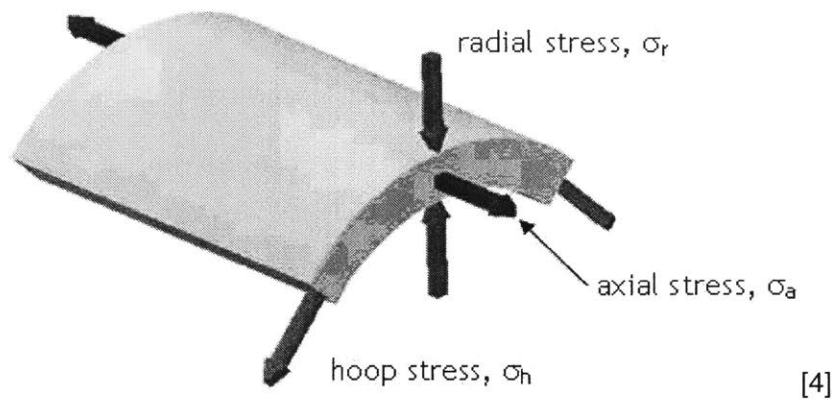


Figure 4-9: Diagram of stress types in a cylindrical model. Radial stress is generally applied throughout the material, but hoop stress only applies to the out ring of the cylinder. There exists a transition point where dominant stress changes from radial stress to hoop stress.

As seen in stress visualization derived from simulation in Figure 4-10, there is a “trough” where vertical stress drops in intensity before it increases again in a sloped manner. This “trough” is the transition point from radial to hoop stress. Also shown in Figure 4-10, the location of the sensors in small footpads are significantly closer to the “trough” than sensors in large footpads. This proximity is likely to affect the results depending on the actual location of this transition region on the physical sensors.

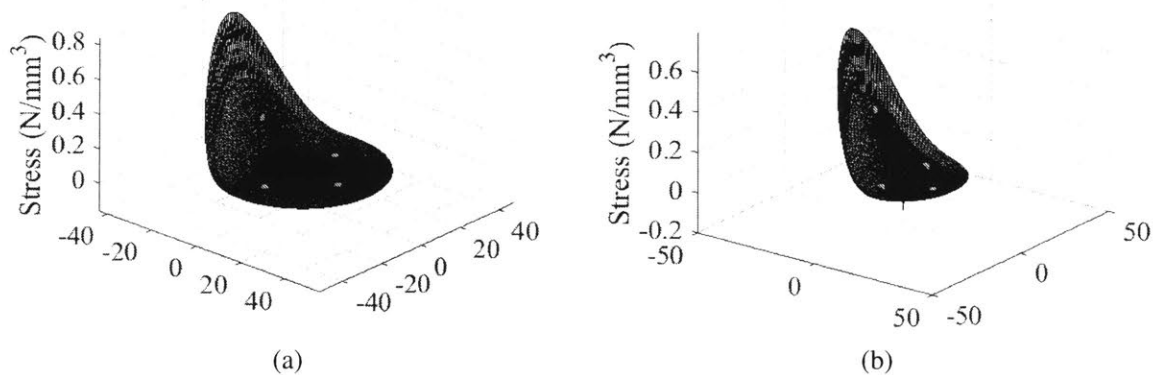


Figure 4-10: (a) Vertical Stress Visualization for large footpad and (b) small footpad compressed 4.5mm at 15 degrees. Red dots indicate location of sensors. A trough is created at the transition point between hoop stress and radial stress dominance. Sensor in small footpad is significantly closer to the trough.

4.2 Rolling:

While angled compression experiments and simulations more accurately capture footpad sensor output at higher contact angles, rolling is preferred for understanding sensor behavior at lower ground contact angles. Rolling from -7 degrees to 7 degrees at 10 different compressions are tested. Models are identified for relating contact angle to applied torque and sensor output. In this section, large and small footpads are analyzed simultaneously as there is little disagreement in the data behavior.

4.2.1 Rolling Experiment:

The most distinctive feature of rolling experiments and simulations is the difference in voltage between sensor 1 and sensor 3, which are located directly opposite of each other and are closest to points of contact, as shown in Figure 4-1. A typical experiment run displays voltage output similar to Figure 4-11. At -7 degrees, sensor 1 peaks in value while sensor 3 has either lifted off or is at its lowest voltage value. At 7 degrees, Sensor 3 reaches peak and sensor 1 either lifts off or is at lowest measured value. Sensor 2 and sensor 4 are generally level in value. Small peaks in voltage value in sensors 2 and 4 are due to imperfect orthogonal orientation of sensor placement. The general decrease in voltage value through each roll is the effect of material stress relaxation. To minimize material stress relaxation effects on experimental results, we performed each experiment three times with two minutes breaks in between. Only the last run is recorded and analyzed. However, since the focus is on voltage outputs of sensor 1 and sensor 3 to characterize each roll, the residue material relaxation effect detected in Sensor 2 and Sensor 4 is not of main concern.

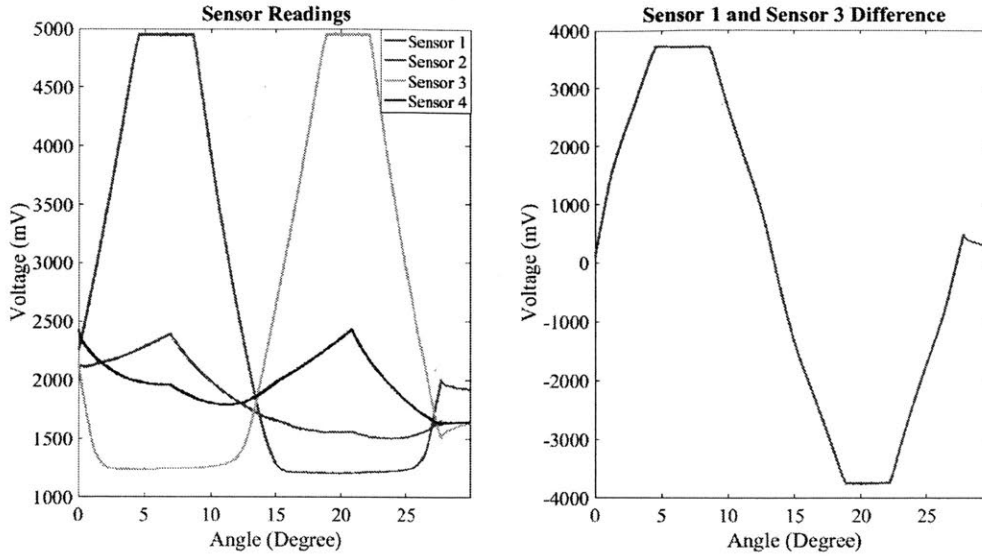


Figure 4-11: Voltage output from sensors embedded in footpads during rolling experiments. Sensor 1 and Sensor 3 exhibit similar behavior with a shifted phase. The flattening of peaks indicate sensors reaching its sensing limit. The flattening of curves at around 1200 mV indicate sensor is no longer in contact with force plate.

The difference between sensor 1 and sensor 3 values is indicative of rolling torque. When graphing the difference between sensor 1 and sensor 3 voltages against experimentally measured torque (data provided by the 6-axis force sensor), there exists a distinct linear correlation that consistent across compressions, as shown by Figure 4-12. The linear fitted trend line of sensor 1 and sensor 3 difference to torque for large footpad is shown in Equation 4-3, and for small footpad is shown in Equation 4-4.

$$V_d = 699.40(\pm 0.40) * t + 18.09(\pm 0.25) \quad (4-3)$$

$$V_d = 1587.0(\pm 0.5) * t + -0.536 (\pm 0.388) \quad (4-4)$$

V_d is the voltage difference between Sensor 1 and Sensor 3 (mV), and t is Torque (N*mm).

Equation 4.3 has a R^2 value of 0.0997, and Equation 4.4 has a R^2 value of 0.0999.

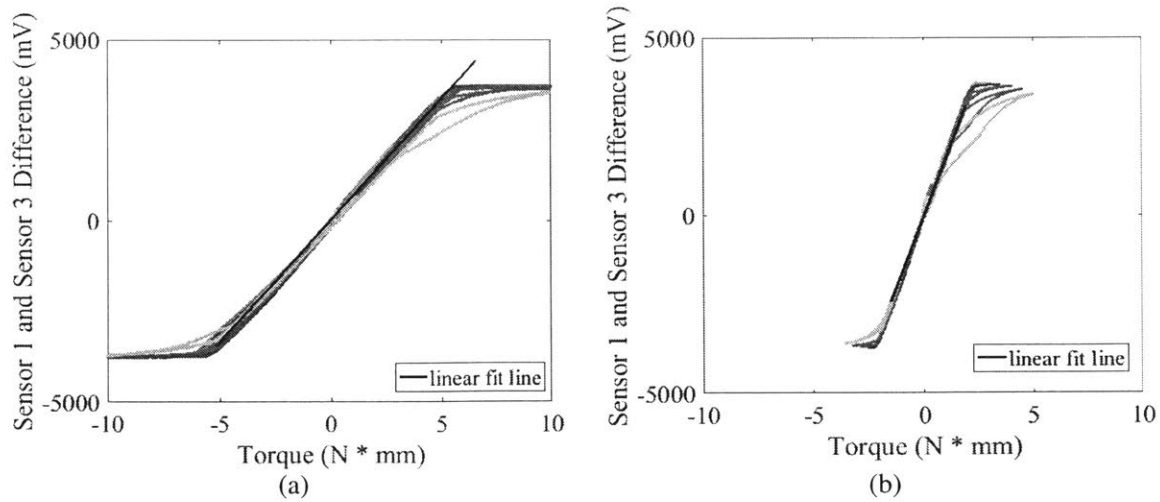


Figure 4-12: (a) The voltage difference between sensor 1 and sensor 3 directly correlates to torque applied to the large footpad, which is shown by the linear relationship between the two factors. (b) The voltage difference between sensor 1 and sensor 3 directly correlates to torque applied to the small footpad, which is shown by the linear relationship between the two factors. The flattening out on both ends are the results of sensors reaching reading limit. The relationship for the large footpad is $V_d = 699.40(\pm 0.40)t + 18.09(\pm 0.25)$, and the relationship for the small footpad is $V_d = 1587.0(\pm 0.5)t + -0.536(\pm 0.388)$, where V_d is the voltage difference between Sensor 1 and Sensor 3 (mV), and t is Torque (N*mm).

When building a model for sensor output across contact angles, we must eliminate effects caused by varying compressions and stress relaxation, and isolate behavior caused by change in angle. Since the effects caused by varying compression and stress relaxation is apparent in sensor 2 and sensor 4 data, we use the average of sensor 2 and sensor 4 data for each compression as the division factor. This combined dimensionless relation will also be referred to as *roll behavior*. Graphing Sensor 1 and Sensor 3 voltage difference divided by Sensor 2 and Sensor 4 voltage average, or roll behavior, for various compressions, we obtain a unique curve for both large and small footpad shown in Figure 4-13.

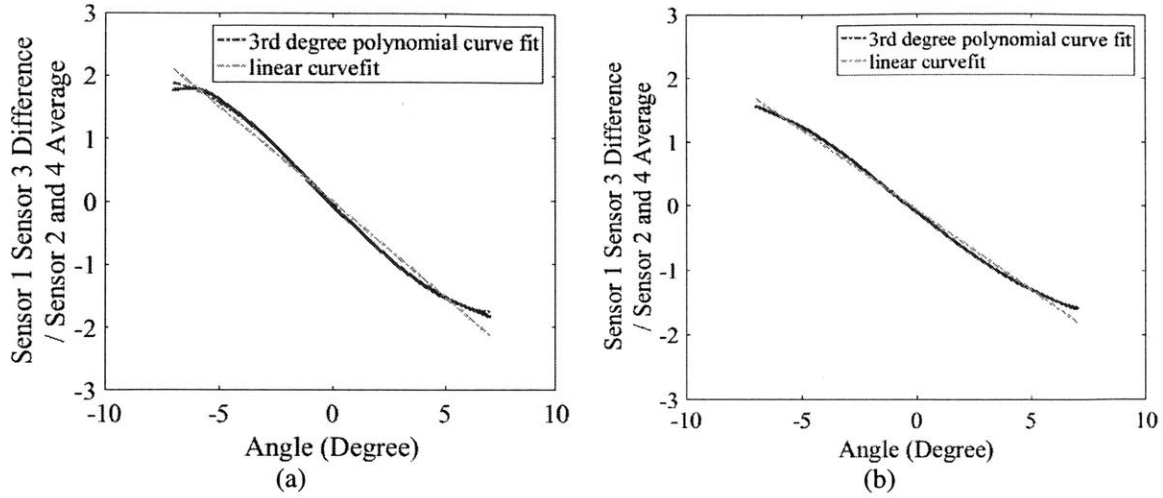


Figure 4-13: (a) Unique curve generated by comparing Sensor 1 and Sensor 3 Difference divided by Sensor 2 and Sensor 4 average voltage (roll behavior) to contact angle for large footpad. (b) Unique curve generated by comparing roll behavior to contact angle for small footpad. Both curves can be fitted with a third degree polynomial function and linear function. The large footpad has a third degree polynomial fitted function of $0.00218(\pm 0.2 * 10^{-4})x^3 + 0.00223(\pm 0.7 * 10^{-4})x^2 - 0.36660(\pm 6.0 * 10^{-4})x + -0.04500(\pm 7.7 * 10^{-4})$ with an R^2 value of 0.9994. The small footpad has a third degree polynomial fitted function of $0.00119(\pm 0.4 * 10^{-5})x^3 + 0.00178(\pm 0.3 * 10^{-4})x^2 - 0.28270(\pm 2.0 * 10^{-4})x - 0.087700(\pm 56.0 * 10^{-4})$. with a R^2 value of 0.9999, where x is the angle in degree. The linear fitted trendline for large footpad is $-0.30300(\pm 5.0 * 10^{-4})x + -0.00853(\pm 20.1 * 10^{-4})$ with R^2 value of 0.9902, and for the small footpad is $-0.2476(\pm 0.3 * 10^{-3})x + -0.0586(\pm 1.1 * 10^{-3})$ with R^2 value of 0.0054.

4.2.2 Rolling Simulation:

A procedure similar to the experiments is simulated in Abaqus FEA. Again, using Equation 2-1 and 2-2 with adjusted parameters, force to voltage conversion in simulation is matched to experimental values. The parameters used are $A = 7.0175$, $B = 0.366$, $\beta = 1570$ for large footpad, and $A = 7.0175$, $B = 0.366$, $\beta = 1570$ for small footpad.

The sensor output to roll contact angle relationship is verified in Abaqus simulation. Figure 4-14 shows simulation results for rolling generally closely match experimental results, therefore we can conclude that model developed for experiment is reliable.

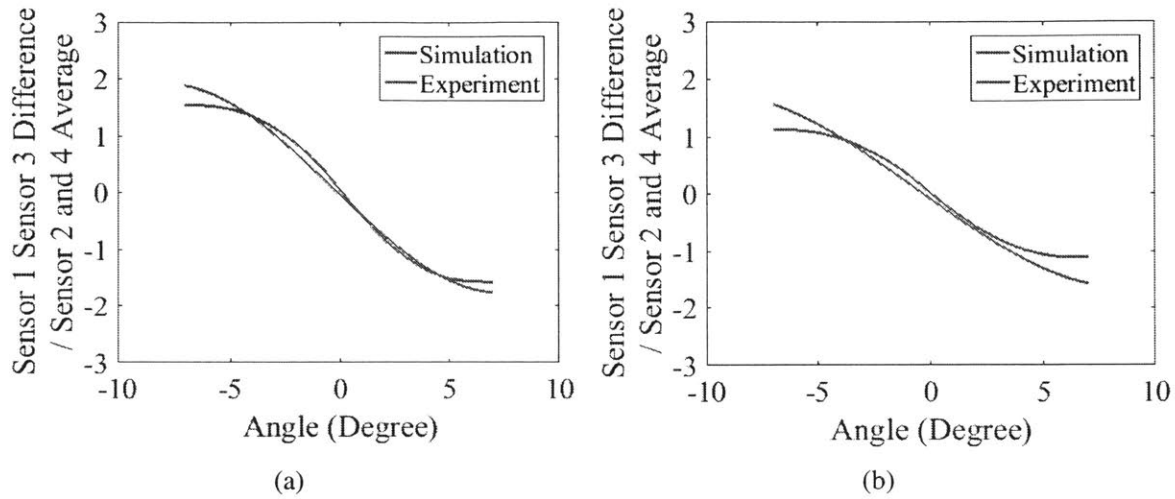


Figure 4-14: (a) Comparison graph between simulation and experimental curves for Sensor 1 Sensor 3 difference/Sensor 2 and Sensor 4 average(roll behavior) to angle (degree) for large footpad. (b) Comparison graph between simulation and experiment curves for roll behavior to angle (degree) for small footpad. This graph confirms our experimental values are valid.

4.2.3 Rolling Comparison and Curve Fit:

From Figure 4-14 we see that simulation for roll behavior appears to be a third degree polynomial fit given the curvature at tail ends. Experiment results, however, is more ambiguous between linear or polynomial fit. Therefore, both linear and third degree polynomial curve fits for experimental data are derived and compared.

Equation 4-5 is the linear fitted trend line for large footpad with R^2 value of 0.9902:

$$roll\ behavior = -0.30300(\pm 5.0 * 10^{-4})x + -0.00853(\pm 20.1 * 10^{-4}) \quad (4-5)$$

Equation 4-6 is the linear fitted trend line for small footpad with R^2 value of 0.0054:

$$\text{roll behavior} = -0.2476(\pm 0.3 * 10^{-3})x + -0.0586(\pm 1.1 * 10^{-3}) \quad (4-6)$$

Equation 4-7 is the characterizing 3rd degree polynomial equation for large footpad with a R^2 value of 0.9994:

$$\begin{aligned} \text{roll behavior} = & 0.00218(\pm 0.2 * 10^{-4})x^3 + 0.00223(\pm 0.7 * 10^{-4})x^2 \\ & - 0.36660(\pm 6.0 * 10^{-4})x + -0.04500(\pm 7.7 * 10^{-4}) \end{aligned} \quad (4-7)$$

Equation 4-8 is the characterizing 3rd degree polynomial equation for small footpad is with a R^2 value of 0.9999:

$$\begin{aligned} \text{roll behavior} = & 0.00119(\pm 0.4 * 10^{-5})x^3 + 0.00178(\pm 0.3 * 10^{-4})x^2 \\ & - 0.28270(\pm 2.0 * 10^{-4})x - 0.087700(\pm 56.0 * 10^{-4}) \end{aligned} \quad (4-8)$$

x is the angle in degree in all equations listed above. All trend lines are plotted against original curve in Figure 4-13.

The third degree polynomial curve fits have uncertainty ranges for all parameters less than 50% of the original value, higher R^2 value than linear fits, and more closely fits the curve-end behavior. Therefore, third degree polynomial curve fit is chosen over linear fit to characterize the relationship between contact angle and roll behavior.

5. Conclusion and Contribution:

This thesis contributes to creating force sensor models and trends for smart shoe footpads used to understand gait contact angle analysis. For both experiments and FEA simulation, angled contact is characterized by angled compression for larger angles, and rolling for smaller angles. In angled compression experiments, angle of contact affects the sensors' voltage to force

conversion rate, with higher angles demonstrating a lower conversion. The modeled relationship between ground force/voltage output is $17.662(\pm 1.790) - 0.306(\pm 0.191) * \varphi$ with R^2 of 0.506, where φ is angle of contact. When observing lower contact angles through rolling experiments, we can identify the torque with the difference in voltage between two embedded sensors in line with direction of roll. The relationship between the two components is $V_d = 699.4(\pm 0.4)t + 18.09(\pm 0.25)$ with R^2 of 0.0997 for large footpad and $V_d = 1587.0(\pm 0.5) * t + -0.536 (\pm 0.388)$ with R^2 of 0.0999 for small footpad, with t as torque, and V_d as sensor voltage difference. The angle of roll can be defined by examining its relationship with the difference in voltage output between two sensors in line of roll divided by the average in voltage output of the two orthogonal sensors, also known as roll behavior. Roll behavior compared across various contact angles is shown in Figure 4-13. The fitted correlation for large footpad is $roll\ behavior = 0.00218(\pm 0.2 * 10^{-4})x^3 + 0.00223(\pm 0.7 * 10^{-4})x^2 - 0.36660(\pm 6.0 * 10^{-4})x + -0.04500(\pm 7.7 * 10^{-4})$ and for small footpad is $roll\ behavior = 0.00119(\pm 0.4 * 10^{-5})x^3 + 0.00178 (\pm 0.3 * 10^{-4})x^2 - 0.28270(\pm 2.0 * 10^{-4})x - 0.087700(\pm 56.0 * 10^{-4})$. Simulation results confirms these trend line behaviors.

These models serve as a starting point for developing more robust contact angle gait analysis with smart shoe footpads. In future works, these trends can be verified with human walking data. Through computer vision trackers, the exact angles of contact that occur during typical walking motion is calculated. Forces are predicted using correlations discovered in this thesis, and verified through FEA simulation. To increase robustness of our model, dynamic implicit simulations may be used to compare simulation stress and experimental forces. Various orientations of sensors should be tested to find the optimal setup for most defining data trends.

In conclusion, a robust model can be developed to associate smart shoe voltage output to distinct angles of contact. These models are crucial to the development of a light and robust system for gait analysis that can help improve athletic performances and medical treatments.

6. References

- [1]Studebaker, S., 2017, “Material Modeling and Sensor Characterization for Optimizing Footpad Force Sensing Array,” Bachelor of Science in Mechanical Engineering, Massachusetts Institute of Technology.
- [2]Bartsch, R., Plotnik, M., Kantelhardt, J. W., Havlin, S., Giladi, N., and Hausdorff, J. M., 2007, “Fluctuation and Synchronization of Gait Intervals and Gait Force Profiles Distinguish Stages of Parkinson’s Disease,” *Physica A: Statistical Mechanics and its Applications*, **383**(2), pp. 455–465.
- [3]Cavanagh, P. R., and Lafortune, M. A., 1980, “Ground Reaction Forces in Distance Running,” *Journal of Biomechanics*, **13**(5), pp. 397–406.
- [4]Kimsey, L., 2017, *What-Is-Radial-Tangential-and-Axial*.
- [5]Wouda, F. J., Giuberti, M., Bellusci, G., Maartens, E., Reenalda, J., Beijnum, V., F. B.-J., and Veltink, P. H., 2018, “Estimation of Vertical Ground Reaction Forces and Sagittal Knee Kinematics During Running Using Three Inertial Sensors,” *Front. Physiol.*, **9**.
- [6]Chuah, M. Y., Romero, J., Ramos, J., and Kim, S., 2018, “Combined Detection of Contact Angle and Ground Reaction Forces for Legged Robots with Point Feet.”